Int. J. Electrochem. Sci., 16 **(2021)** Article ID: 210829, doi: 10.20964/2021.08.12

International Journal of
ELECTROCHEMICAL
SCIENCE
www.electrochemsci.org

Highly sensitive Electrochemical Sensor based on Perovskite type $PrCoO_3$ for the detection of carbendazim

Ruspika Sundaresan[1], *Vinitha Mariyappan*[1], *Tse-Wei Chen*[2], *Shen-Ming Chen*[1,*], *Naveen Karuppusamy*[1], *Muthumariappan Akilarasan*[1]

[1] Department of Chemical Engineering and Biotechnology, National Taipei University of Technology, No.1, Section 3, Chung-Hsiao East Road, Taipei 106, Taiwan.
[2] Department of Materials, Imperial College London, London, SW7 2AZ, United Kingdom
[*]E-mail: smchen1957@gmail.com, smchen78@ms15.hinet.net

Received: 2 April 2021 / *Accepted:* 30 May 2021 / *Published:* 30 June 2021

In this work, the Carbendazim fungicide was detected using an electrochemical sensing platform based on the Praseodymium cobalt oxide (PrCoO3) compound, which was synthesized using a simple co-precipitation process. Field emission scanning electron microscopy (FESEM), energy dispersive X-ray (EDX), powder X-ray diffraction (XRD), and X-Ray photoelectron spectroscopy (XRPS) were used to classify the synthesized content.The electrical conductivity of $PrCoO_3$ was investigated by using electrochemical impedance spectroscopy. $PrCoO_3$ compound were used to detect CBZ. Cyclic voltammetry and differential pulse voltammetry were used to scrutinize the electrochemical performance of CBZ on $PrCoO_3$/GCE.The electrocatalytic operation of the prepared sensor against CBZ was exceptional. Additionally, under streamlined laboratory conditions, the PrCoO3 sensor has a higher sensitivity of 9.6619 A M1 cm2, a lower detection limit (LOD) of 2 nM, and a linear range of 0.001 to 84 M for CBZ detection. Furthermore, the effect of storage time on the PrCoO3 sensor's CV response reveals a higher stability.The as-fabricated sensor was successfully used to detect the CBZ level in orange juice and river water due to its exceptional analytical benefits.

Keywords: Carbendazim, co-precipitation, electrochemical sensor, cyclic voltammetry.

1. INTRODUCTION

Nowadays, the increased use of poisonous pesticides is a significant environmental issue. Carbendazim (CBZ) is a systemic benzimidazole fungicide and is mainly used in agriculture, forestry, and veterinary medicine[[1]]. CBZ is a significant pollutant found in fruit, soil, and water[2]. CBZ's prolonged and repeated application causes acute and delayed toxic effects in mammals, invertebrates, and marine life[3]. The ring on CBZ is hard to break with slow degradation[4]. It is both a metabolite and breakdown product of benomyl product of thiophanate methyl in plants and the environment[5].

Under normal environmental conditions, it is very stable for a long time and it has been frequently detected in surface water[6]. Maximum residue limits (MRLs) for carbendazim in citrus have been set by the European Union, ranging from 100 to 700 ppb. [7]. The World Health Organization has listed CBZ as a toxic chemical. CBZ and carbonyl have been identified as potential human carcinogens[8]. CBZ has been banned in Australia, the majority of the European Union, and the United States due to its extreme toxicity and persistence[9]. However, the United Kingdom, Portugal and developing countries such as Brazil, China, and India continue to allow the manufacture and use of carbendazim in different formulations[10]. Repeated use of CBZ causes growth and degradation in different habitats, with long-term impacts on quality of soil, human and animal health[11]. Various methods are already in practice to determine the carbendazim such as high-performance liquid chromatography[12], mass spectroscopy[13], resonance energy transfer[14], impedimetric aptasensor[15], fluorescence[16], colorimetry[17], and dispersive liquid-liquid micro extraction[18]. Compared with traditional analytical methods electrochemical technique is cheap, rapid, robust, selective, and highly sensitive[19]. Therefore, numerous electrochemical sensors were reported for the detection of CBZ with different nano-composite-modified electrodes. Yujing Guo et.al reported cyclodextrin-graphene hybrid nanosheets exhibited a good linear range of 5 nM–0.45 μM and limit of detection (LOD) 2 nM[20]. Rongjing Cui group developed phosphorus-doped helical carbon nanofibers for the CBZ detection and they reported the LOD is 0.038 μM.

An electrochemical sensor for the detection of biological molecules and heavy metals, metal, semiconductor nanocrystal, and other electroactive nanoparticles are routinely employed[21]. These electroactive nanoparticles may be deposited on the electrode, which producing strong and stable electrochemical signals[22]. Perovskite type compounds have been considered potential materials in recent decades due to their properties interrelated to high-temperature superconductivity[23], magnetoresistance[24], dielectric properties[25], ionic conductivity[26], solid-oxide fuel cells (SOFC)[27], membrane separation[28], sensors[29], catalysis[30], and many other applications. Praseodymium cobaltite ($PrCoO_3$) perovskite-type oxide is an important material[31], Because of their intriguing magnetic properties, they have recently sparked a lot of research interest.

In this study, we successfully prepared $PrCoO_3$ compound by simple co-precipitation assisted calcination method. Further, $PrCoO_3$ compound were used as electrode material for CBZ detection. The formation of a Praseodymium cobaltite was confirmed by FE-SEM, XRD, and XPS techniques. As prepared $PrCoO_3$ compound would modify the working electrode (GCE) surface for detection of CBZ. The proposed sensor provides high selectivity, great sensitivity, and quick response to detect CBZ in orange juice and river water. Here in this work, we report the modified electrode of $PrCoO_3$ to have a great electrode active surface area and high electrical conductance for the detection of Carbendazim.

2. EXPERIMENTAL SECTION

2.1. Materials and Reagents

Praseodymium (III) nitrate hexahydrate ($Pr(NO_3)_3.6H_2O$,99.9%), Cobalt (II) nitrate hexahydrate ($Co(NO_3)_2.6H_2O$,≥98%), ethylene glycol ($(C_2H_6O_2)$, 99.8%), urea ((CH_4N_2O), 99.0-100.5%) and

carbendazim, ($C_9H_9N_3O_2$, 97%) Sodium hydroxide (NaOH, 98%), hydrochloric acid (HCl, 36.5–38.0%), potassium chloride (KCl, 99.0-100.5%), potassium ferrocyanide $K_4[Fe(CN)_6]$, potassium ferricyanide $K_3[Fe(CN)_6]$, were purchased from Sigma Aldrich have been used without further purification. Double distilled (DD) water and ethanol were used throughout the experiments for solution preparation and other purposes. Phosphate buffer (0.1M) solution was prepared by mixing the $NaH_2PO_4.H_2O$, $NaHPO_4$ in DD water, and the pH was adjusted by using NaOH (0.1M) and HCl solution. All of the chemicals used in these experiments were of standard analytical grade, and the electrochemical experiments were carried out at room temperature in a deoxygenated atmosphere. Orange juice was purchased in Taipei local market and a river sample was collected from the Xindian river for real sample analysis.

2.2. Material Characterization

The morphology and the structure of the as-synthesized material were analyzed by using Field emission electron microscopy (FESEM, Hitachi S-3000). The XRD pattern of material was recorded on (XRD, X'Pert- PRO, PANanaytical B.V., and The Netherland). The composition and chemical state of the catalyst was analyzed by X-ray photoelectron spectroscopy (XPS, Thermo ESCALAB 250). The electrochemical measurements were verified by using a three-electrode system. It consists of a glassy carbon electrode (surface area 0.071 cm^2) as a working electrode, platinum wire as a counter electrode, Ag/AgCl as a reference electrode. The electrochemical experiments were carried out in an electrochemical workstation cyclic voltammetry (CV CH1205C) and differential pulse voltammetry (DPV CHI900) in the potential range of +0.5 to +1.2 (Ag/AgCl vs V) at a scan rate of 50 mVs^{-1}. The Nyquist plot was obtained by electron impedance spectroscopy (EIS).

2.3. Synthesis of $PrCoO_3$

For the synthesis of $PrCoO_3$, 1.305 g of $Pr(NO_3)_3.6H_2O$, 0.873 g of $Co(NO_3)_2.6H_2O$ were dispersed into 50 ml of DD water stirred under a magnetic stirrer for 30 minutes. Then 10 ml of ethylene glycol and 0.5 g of urea were added to the reaction mixture and continuously stirred for 1hour. The obtained precipitate was centrifuged with DD water and ethanol several times, then the sample was dried at 80˚C and calcined at 650˚C for 4 hours the resultant powder was named $PrCoO_3$.

2.4. Modification of glassy carbon electrode:

The GCE surface was polished with 0.05µm of α-alumina (α-Al_2O_3) powder over the silicon carbide paper and rinsed under the DD water flow on the GCE surface, along with ethanol wash and dried. Later, 1mg of as-prepared material dispersed in 2 ml of water and sonicated for 20 minutes. 6 µL of composite suspension was loaded on GCE surface by drop cast method and it was dried in an oven at 50°C for 20 minutes. Further used for the electrochemical investigation.

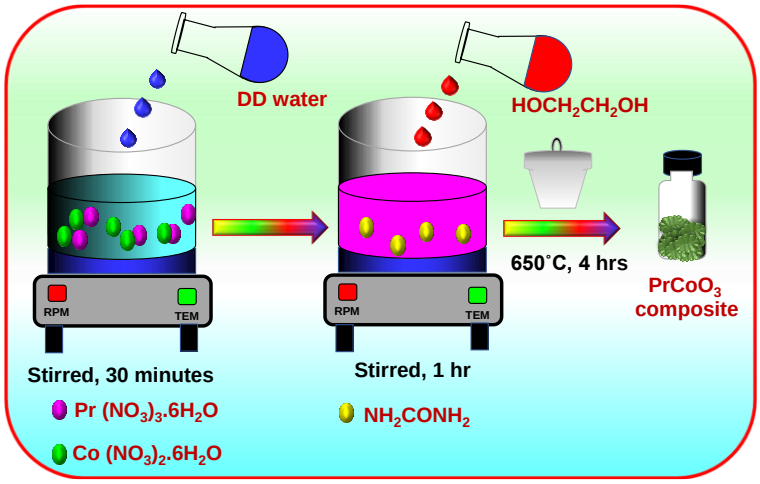

Scheme 1. Preparation of $PrCoO_3$ by co-precipitation assisted calcination method.

3. RESULT AND DISCUSSION

3.1. Morphological characterization of $PrCoO_3$

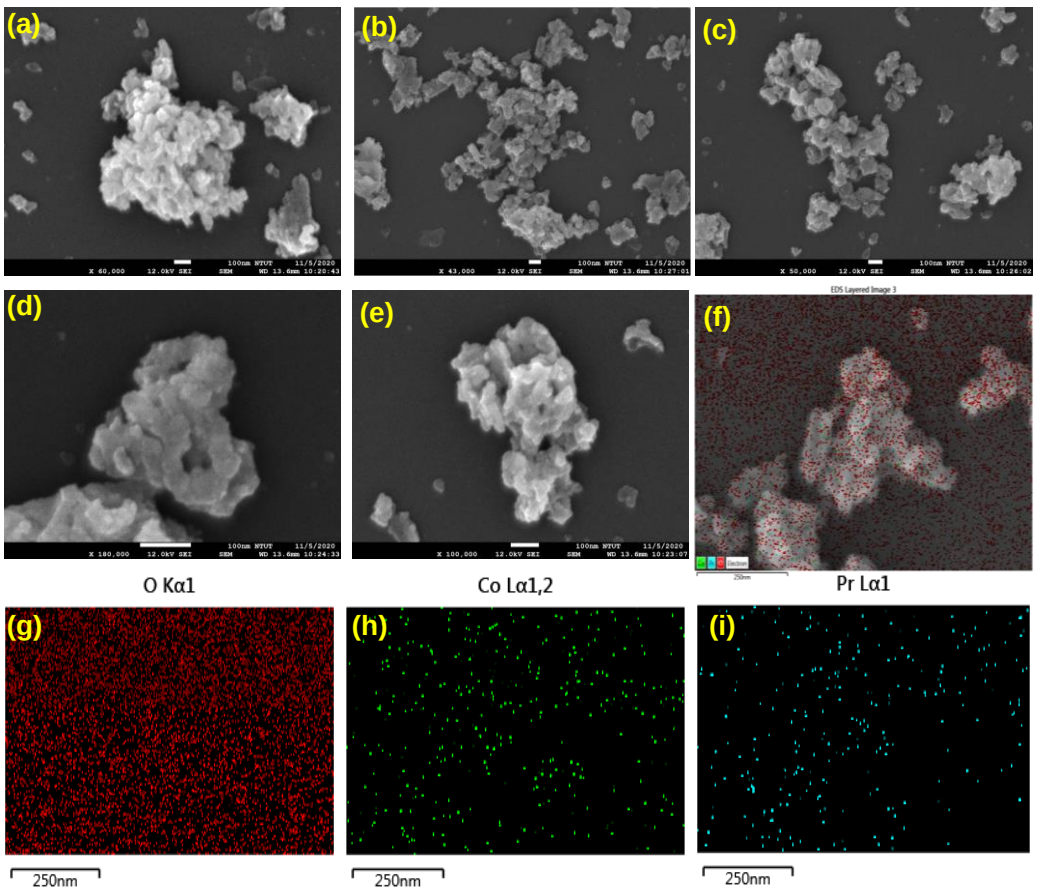

Figure 1. (a-e) High magnifying FESEM image of $PrCoO_3$, (f-i) FESEM-EDS mapping of $PrCoO_3$ (f) mixed color of Pr, Co, O (g) O (red dots), (h) Co (green dots), (i) Pr (blue dots).

The Field emission scanning electron microscopy (FESEM) was used to examine the morphology of the $PrCoO_3$ compound. Fig1. (a-e) shows the FESEM images of $PrCoO_3$ which indicates the synthesized material has a nanoflake structure with a well-defined smooth surface. The compound of $PrCoO_3$ were slightly aggregated and irregularly arranged. The particles are not formed uniformly, Image processing software was used to determine the size distribution of the compound (Image J). The average particle size is 80-120nm.Fig.1. (f-i) shows the EDS mapping of the $PrCoO_3$ compound, it confirmed that the presented elements are equally distributed in the $PrCoO_3$ compound. Fig.2. shows the EDS-spectrum Pr, Co and O were presented with 28.2.32.5 and 39.3%, respectively.

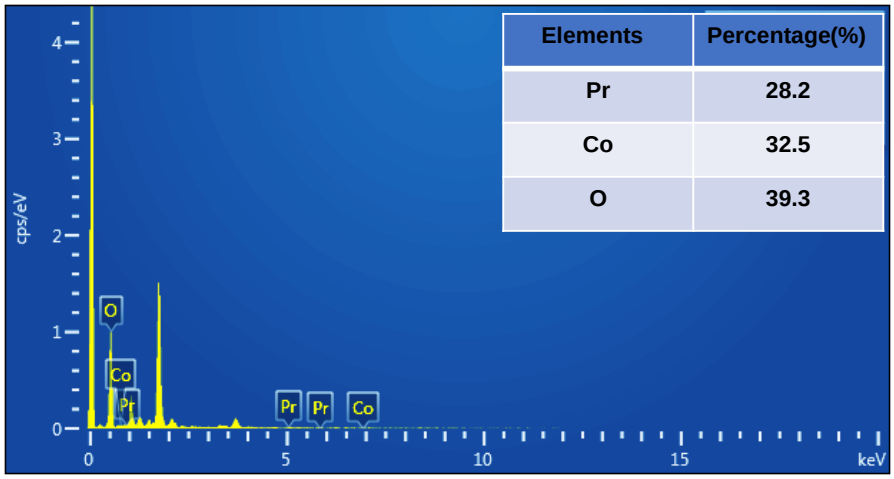

Figure 2. FESEM-EDS spectrum of $PrCoO_3$ insert; the elemental percentage of Pr, Co, O.

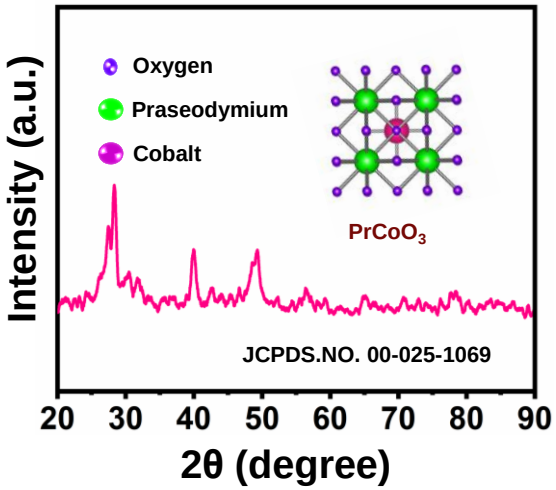

Figure 3. XRD pattern of $PrCoO_3$.

The X-ray diffraction pattern of $PrCoO_3$ compound was shown in fig.3. XRD pattern of $PrCoO_3$ exhibits narrow peak with high-intensity diffraction pattern of 2θ angle at, 26.26, 33.45, 48.02, 49.61, 59.76, 71.52, and 80.06. The 2θ values are corresponding to the planes (210), (220), (400), (410), (422), (441), and (620). The obtained diffraction peaks of $PrCoO_3$ were coordinated with the previously reported XRD pattern of JCPDS.NO.00-025-1069[32]. The particle size was determined by the Debye-

Scherrer equation. ($D=K\lambda/(\beta\cos\theta)$; λ is the wavelength of Cu-Kα= 1.54178 Å, D is the size of the crystallite; K is the Scherrer constant =0.89, θ is the XRD peak position, β is the full width at half-maximum (FWHM). The average particle size of the $PrCoO_3$ was calculated as ≈ 100 nm. The narrow peak indicates that as prepared $PrCoO_3$ compound were highly pure and have a good crystalline order.

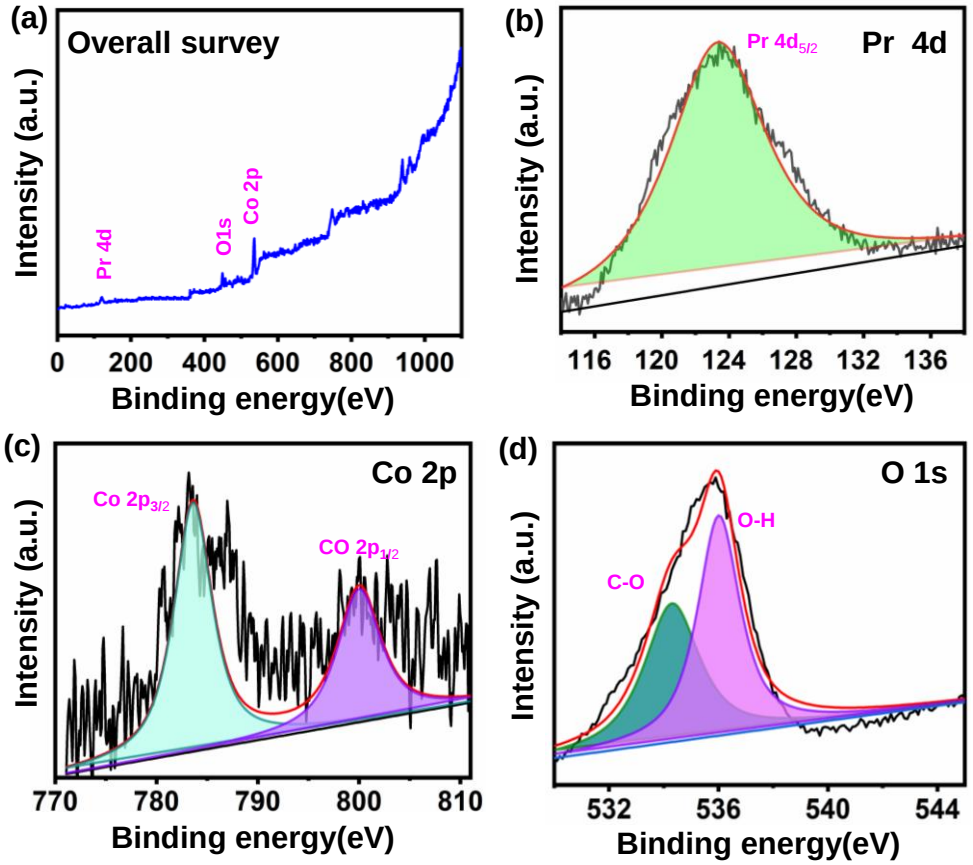

Figure 4. (a) XPS overall survey spectra of $PrCoO_3$. (b) High-resolution spectra of Pr 4d, (c) Co 2p, (d) O 1s.

The chemical composition and chemical state of the as-synthesized compound were analyzed by the XPS. Fig.4 (a) shows the overall survey spectrum of $PrCoO_3$ indicates the presence of Co, O, and Pr. Fig.4. (b) shows the high-resolution spectrum of Pr the peaks found at 123.5 eV attributed to 4d energy state. The obtained results have shown that the existence of Pr^{2+} [33]. Fig.4(c)shows the XPS spectrum of Co 2p spectra two strong peaks at 783.2 and 801eV, which attributes to 2 $p_{3/2}$ and 2 $p_{1/2}$ [34]. Fig.4(d) shows The O 1S spectrum shows two peaks at 534.3 and 536 eV[35]. The obtained results confirmed the presence of Pr 4d, Co 2p, and O 1s in the $PrCoO_3$.

3.4 Electrochemical impedance spectroscopy (EIS)

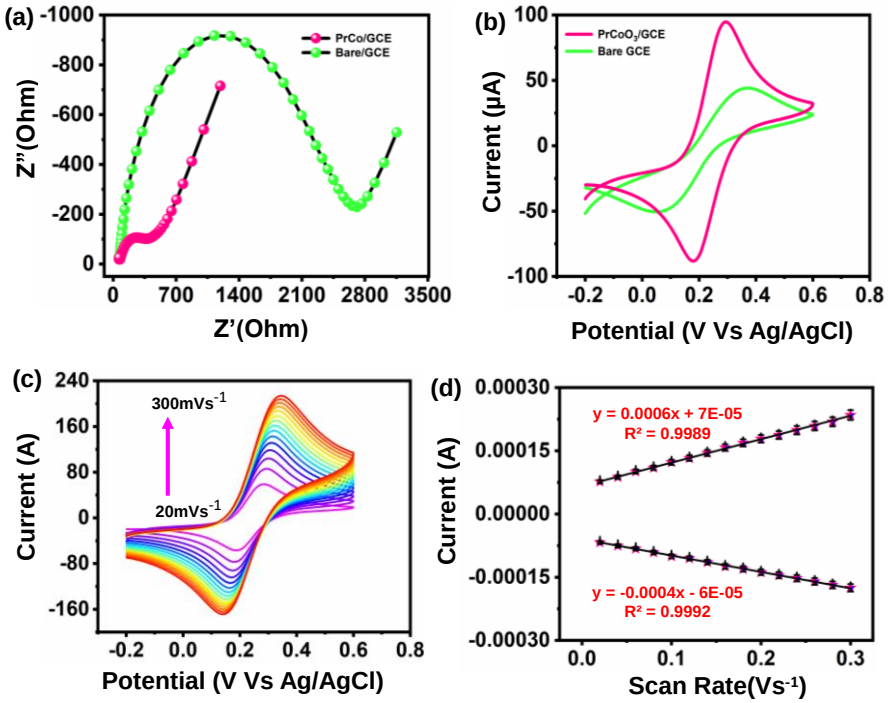

Figure 5. (a) EIS spectra of bare GCE, $PrCoO_3$/GCE, (b) CV response of bare GCE, $PrCoO_3$/GCE at a scan rate 50 mV s^{-1}, (c) CV response of $PrCoO_3$/GCE at scan rate from 20 to 300 mV s^{-1}, and (d) fitted curves of current response versus scan rates. All these experiments were carried out in 5 mM $[Fe(CN)_6]^{3-/4-}$ containing 0.1 M KCl solution.

The EIS technique is used to examine the charge transfer kinetic parameter of a synthesized electrocatalyst material. The EIS analysis was done for the bare GCE, and $PrCoO_3$/GCE in 0.1M KCl solution containing 5 mM of $K_3[Fe(CN)_6]$ and $K_4[Fe(CN)_6]$, and the equivalent Nyquist plot are displayed in (Fig. 5a). The charge-transfer resistance (Rct) owing to the faradic reaction between the electrode and the electrolyte is described by the semicircle observed in the higher frequency region and the diameter of the semicircle. The charge transfer resistance ($R_{c)t}$ values were calculated to be, 2604.21and 318.64Ω for bare GCE, and $PrCoO_3$/GCE respectively. The attained results display that the $PrCoO_3$ modified electrode has high electrical conductivity as compared to the bare GCE, this result showed that the $PrCoO_3$ modified GCE has a more active site compared to the bare GCE.

Also, cyclic voltammetry (CV) was used to attain a better understanding of the $PrCoO_3$ compound, as shown in Fig.5b. The $PrCoO_3$ compound have a higher electrochemical redox peak current than bare GCE. Because of its large specific surface area and expanded number of active sites, PrCoO3 exhibits extraordinary electrocatalytic behavior, resulting in a strong redox peak present.. The $PrCoO_3$ modified electrode has the highest redox peak current value (Ip) and a smaller peak-to-peak separation (ΔE_p) than the bare GCE; The higher (I_p) and lower ΔE_p of $PrCoO_3$ suggest rapid electron transfer in the $[Fe(CN)_6]^{3-/4-}$ system.

The catalytic kinetics of the $PrCoO_3$ compound was investigated at various scan rates ranging from 20 to 300 mV s^{-1}. As shown in Fig.5c, When scan rates were raised from 20 to 300 mVs-1, the

PrCoO3 redox peak current rose, revealing the polarization curve of the aqueous electrolyte and the rapid kinetics of the electrode.Fig. 4d. shows a linear plot of I_{pa} and I_{pc} peak current versus the square root of the scan rate, with coefficients (R^2) of 0.9989 and 0.9992, respectively. The Electrode Active Surface Area (EASA) of the $PrCoO_3$/GCE was calculated using the Randles–Sevcik equation (1)

$$I_{pa} = (2.69 \text{ X}10^5)\, n^{3/2}\, \text{ACD}^{1/2}\, v^{1/2} \qquad (1)$$

Where A is the active surface area of the electrode, I_{pa} is the peak current value, D is the electrolyte diffusion coefficient, C is the ferricyanide solution concentration, n is the total number of electrons involved in the reaction, and μ is the scan rate (V s^{-1}). From the slopes of I_{pa} vs. square root of scan rate (mV s^{-1}) the EASA was calculated shown in Fig. 5d. The measured EASA for the bare GCE, $PrCoO_3$/GCE were 0.146 and 0.235cm^2 respectively. The higher EASA of $PrCoO_3$/GCE is predicted to support the electrochemical reaction with CBZ.

3.4. Electrochemical detection of CBZ

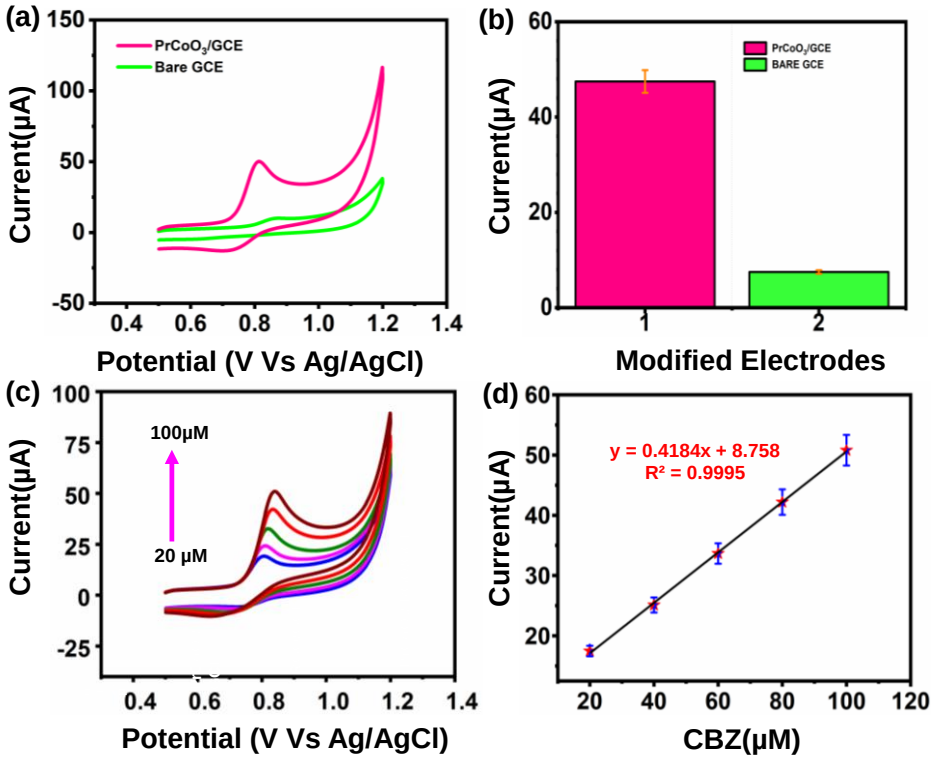

Figure 6. (a) CV responses of bare GCE, and $PrCoO_3$/GCE in the presence of 100 μM CBZ with 0.1 M PB (pH 7.0) at a scan rate 50 mV s^{-1}, (b) the dependence bar diagram for oxidation peak current response for CBZ over different bare GCE and, $PrCoO_3$/GCE (c) CV responses of $PrCoO_3$/GCE at different concentration of CBZ (20-100 μM) with 0.1 M PB (pH 7.0) at a scan rate 50 mV s^{-1}. (d) The dependence linear calibration plot for oxidation peak current Vs concentration of CBZ.

The electrocatalytic behavior of CBZ was investigated by using cyclic voltammetry. Fig.6.(a) shows the cv performance of bare GCE and $PrCoO_3$/GCE_3 in 100μM of CBZ with a 0.1M PB (pH=7.0) solution at a scan rate of 50mVs^{-1}. The bare GCE shows low anodic peak current intensity for the electrochemical detection of CBZ. $PrCoO_3$/GCE shows a higher peak current intensity for CBZ. In the

case of, $PrCoO_3$ the higher surface area of the nanoflake structure one of the main reasons behind the electrochemical performance towards CBZ. Fig.6. (b) shows the corresponding bar graph for current versus bare GCE and $PrCoO_3$/GCE.

Fig. 6(c) shows a cv curve of $PrCoO_3$/GCE at different concentration (20-100µM) in 0.1M PB (pH=7.0) solution at a scan rate 50 mVs^{-1}. The redox peak current intensity of CBZ gradually increases with the increase in concentration from 20-100 µM which implies the rapid electron transfer rate of $PrCoO_3$/GCE compound. Fig.6(d) shows the relationship between the peak current and concentration shows linearity with a regression equation I_{pa} = 0.4184[CBZ]/(µM) + 8.758 and R^2 = 0.9995 respectively. This result reveals that $PrCoO_3$/GCE possesses good electrochemical sensing for CBZ.

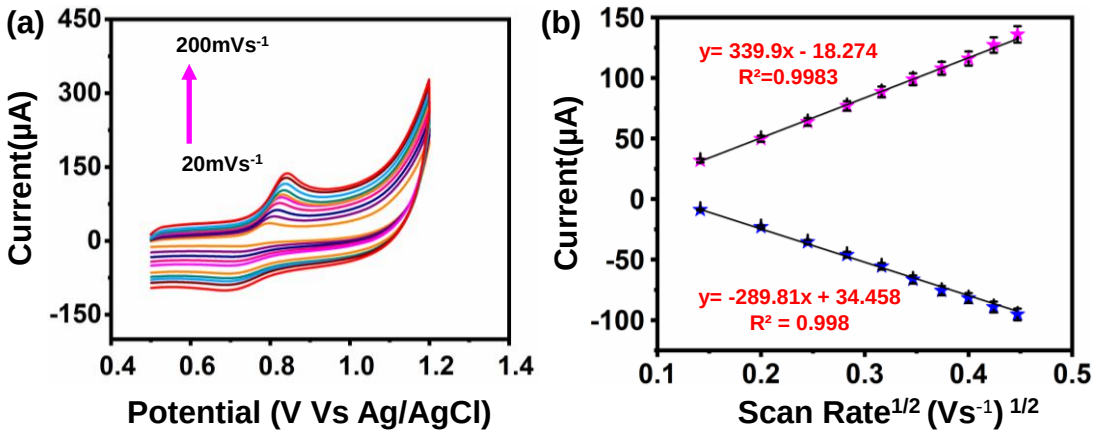

Figure 7. (a) CV response of $PrCoO_3$/GCE at different scan rates (20-300 mVs^{-1}) in deoxygenated 0.1 M PB (pH 7.0) contained 100 µM of CBZ. (b)The dependence plot for peak current versus scan rates.

The electrocatalytic kinetic behavior of $PrCoO_3$/GCE was investigated by performing varied scan rates by cv analysis. Fig 7(a) shows the cv response of $PrCoO_3$ /GCE in 100µM at varying scan rates (20-200mVs^{-1}). The peak current progressively increases with a increase in scan rate and the obtained plot indicates a good linear relationship between scan rate and current I_{pa}. Fig.7. (b) shows the linear aggression equation of I_{pa} = 339.9(V s^{-1}) - 18.274 and R^2= 0.9983 exhibits a surface adsorbed-controlled process.

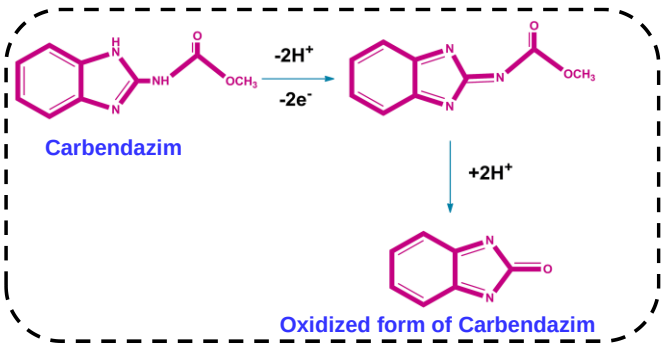

Scheme 2. Electrochemical oxidation of carbendazim over $PrCoO_3$/GCE.

3.6 DPV analysis of CBZ

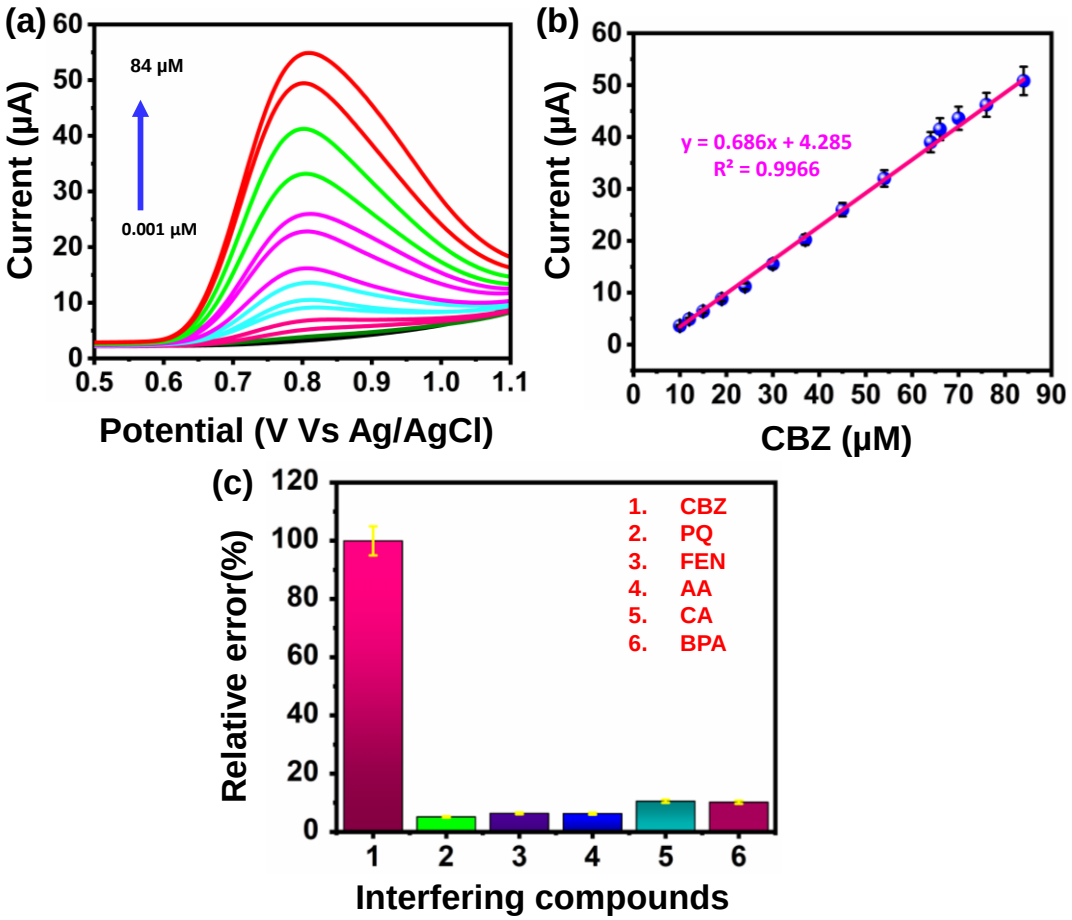

Figure 8. (a) DPV response of the $PrCoO_3$/GCE with different concentration of CBZ (0.001-84 µM) in deoxygenated 0.1 M PB (pH 7.0), (b) the dependence linear plot for peak current response versus concentration of CBZ (c) The bar diagram of relative error (%) of current versus interfering molecules.

DPV analysis was used to inspect the reliability of the $PrCoO_3$/GCE sensor for CBZ detection. Fig. 8a shows the DPV response of $PrCoO_3$/GCE towards continuous injection of various concentrations of CBZ (0.001–84 µM) under deoxygenated 0.1 M PB (pH 7.0). We observed after each addition of CBZ the anodic current response increases rapidly. The obtained current response of $PrCoO_3$/GCE was linearly scaled with the wide concentration of CBZ showed in Fig. 8b. The linear regression equation could be expressed as I_{pa} (µA) = 0.686 [CBZ] (µM) +4.285 and the coefficient (R^2) of 0.9966. The limit of detecting (LOD) was calculated to be 0.002 µM by the standard equation, LOD = 3 S/q. where 'q' is the slope value (0.686 µA μM^{-1}) from the calibration plot, and 'S' is the standard deviation obtained from the five measurements of the blank signal (0.00062729 µA). Meanwhile higher sensitivity was obtained to be 9.6619 µA μM^{-1} cm^{-2}. Moreover, the analytical parameters of the $PrCoO_3$/GCE sensor for CBZ sensing were compared with those of other reported CBZ sensors in terms of linear range, sensitivity, and LOD as shown in Table 1. It can be noted that the LOD and linear range of the suggested

$PrCoO_3$/GCE sensor was lower LOD and broader linear range than those of previously reported CBZ sensing materials.

Table 1. Comparisons of the $PrCoO_3$/GCE linear range, sensitivity, and limit of detection with the previously reported electrodes for electrochemical detection of CBZ.

Electrodes	LOD (µM)	Linear range(µM)	Method	Reference
[a]GW Nfs/[b]SPCE	0.005	0.02−40	DPV	[36]
$ZnFe_2O_4$/[c]SWCNTs/[d]GCE	0.09	0.5−100.0	DPV	[37]
[e]GS/GCE	0.00078	0.005–1.57	DPV	[38]
[f]CPE/[g]FS@Ag	0.00094	0.05-3.0	DPV	[39]
[h]GdO NRs/[i]GA	0.003	0.01−75.00	DPV	[40]
[j]ILs-$CaFe_2O_4$/[k]MWCNTs/GCE	0.00941	0.0523-105	DPV	[41]
MXene/[l]CNHs/[m]β-CD-MOF /GCE	0.001	0.003 - 10.0	DPV	[42]
[n]CMC-MWCNTs/GCE	0.015	0.03-10	DPV	[21]
La-Nd_2O_3/CPE	0.027	0.08–50	DPV	[43]
$PrCoO_3$/RGO	0.002	0.001-84	DPV	This work

[a]gadolinium tungstate compound;[b]SPCE: screen-printed carbon electrodes; [c]SWCNTs: Single walled carbon nanotubes;[d]glassy carbon electrode; [e]GS/GCE:graphene nanosheet; [f] CPE : Carbon paste electrode; [g]silver nanoparticles on fumed silica;[h]gadolinium oxide nanorods [i]GA: graphene aerogel;[j] Ionic liquids; [k]MWCNTs: Multi-Walled Carbon Nanotubes; [l]CNH: carbonnanohorns;[m]β-cyclodextrinMetal-organic frameworks; [n]carboxymethyl cellulose;

3.7 Effect of interference

The anti-interference capability of an electrochemical sensor is a noticeable analytical parameter to their practical analysis. Under a physiological condition, the effect of other electroactive species is commonly obtained at an applied working potential. Hence, selectivity of as-fabricated $PrCoO_3$/GCE was studied with the DPV technique against consecutive injection of 100 µM CBZ and 10-fold excess concentration of interferences interfering agents such as paraquat (PQ), fenamiphos (FEN), ascorbic acid (AA), citric acid (CA), bisphenol A (BPA), under deoxygenated 0.1 M PB (pH 7.0. From the DPV responses, the peak current response and peak potential were unaffected by the inclusion of a 10-fold excess concentration of interferences. Moreover, no additional peak responses were observed for added interferences. The corresponding relative error (%) of current recovery versus interfering specious was given in Fig.8c and the recovery current of CBZ was obtained in the range of 92.5-98.5 %. The obtained

results indicate the excellent selectivity of the $PrCoO_3$/GCE sensor for the electrochemical oxidation of CBZ.

3.8 Stability and Reproducibility

Fig.9a shows the bar diagram of 5 different electrodes versus the current response towards 100 µM of CBZ in deoxygenated 0.1 M PB (pH 7.0), relative standard deviation (RSD) was calculated to be 2.53 %, which shows the excellent reproducibility of the $PrCoO_3$/GCE electrode.

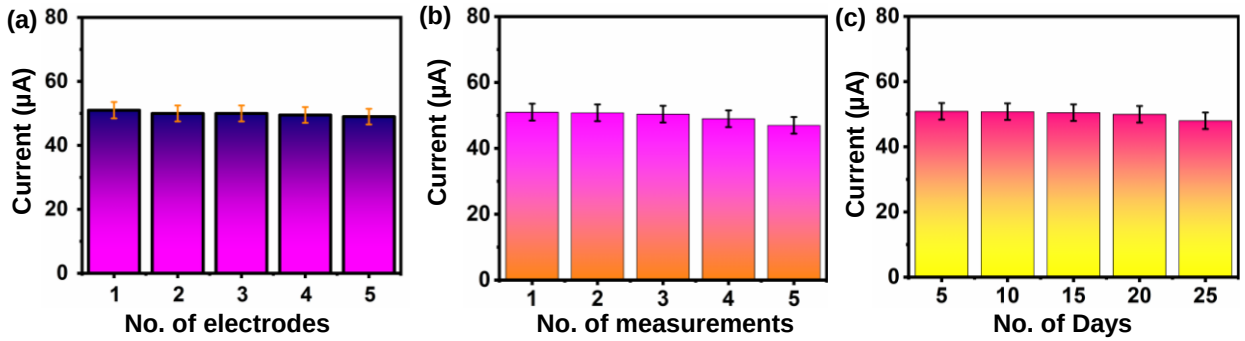

Figure 9. (a) The bar diagram for the current response of 5 independent $PrCoO_3$/GCE at 100 µM of CBZ in deoxygenated 0.1 M PB (pH 7.0) at a scan rate of 50 mV s^{-1}, and (b) The bar diagram for the current response of single $PrCoO_3$/GCE for five repetitive measurements in 100 µM of CBZ in deoxygenated 0.1 M PB (pH 7.0) at a scan rate of 50 mV s^{-1}.(c) The bar diagram for the long-term stability of the $PrCoO_3$/GCE over 25 days.

The repeatability of the $PrCoO_3$/GCE electrode was explored by five consecutive repeatable measurements using a single $PrCoO_3$/GCE electrode in 0.1M PB (pH 7.0) containing 100 µM CBZ. The bar diagrams depicted in Fig. 9b show the current response of the $PrCoO_3$/GCE electrode for repeatable measurement of CBZ and the RSD is calculated to be 2.26%, evident of the excellent repeatability of the $PrCoO_3$/GCE electrode. The lasting electrochemical stability of the $PrCoO_3$/GCE sensor was evaluated by CV response of $PrCoO_3$/GCE electrode towards 100 µM of CBZ in 0.1 M PB (pH 7.0) for 25 days displayed in Fig. 9c, the current responses have been measured every 5 days intervals after the electrode is stored in the refrigerator at 4° C. The $PrCoO_3$/GCE electrode retained 95.4 % of current from its first day and the RSD value is 2.32 %, the obtained result revealed the outstanding long-term stability of our proposed $PrCoO_3$/GCE electrode. These results evidence that perovskite-type nanoparticles provide structural stability and a high surface area to the $PrCoO_3$.

3.8. Real sample analysis

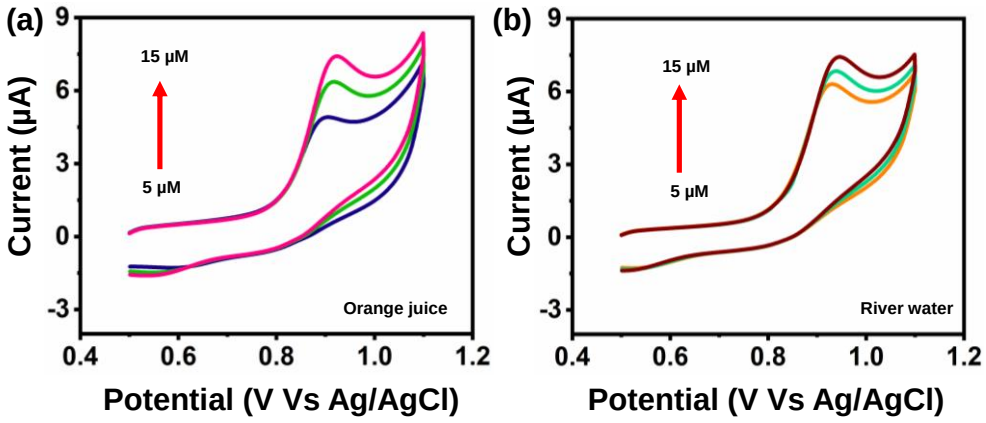

Figure 10. CV response of spiked CBZ in (a) orange juice (b) river water.

To evaluate CBZ in the orange juice and river water samples (Fig.10a and b), the practical application of the fabricated sensor was evaluated. The orange juice sample was bought from a Taipei local market and river water was collected from the Xindian river, diluted 20 times in deoxygenated 0.1 M PB (pH 7.0). A known concentration of CBZ was added to the pre-treated real samples in CV analysis under optimum conditions by the standard addition method. The prepared $PrCoO_3$/GCE sensor to detect the concentration of CBZ in different samples before and after spiking, the obtained results are summarized in Table.2. The results showed that the recoveries varied from 99.8% to 101.6%, were excellent, which exposed that the prepared sensor can be used as an effective and reliable sensing platform for CBZ determination in real samples. It's conceivable that the prepared sensor would be able to detect CBZ in both commercial and lab samples, with reasonable recovery rates. Finally, these findings support the hypothesis that the proposed sensor can be used to determine CBZ in real samples in a convenient, accurate, sensitive, and feasible manner.

Table 2. Determination of CBZ in orange juice and river water sample at $PrCoO_3$/GCE.

Real samples	Added (µM)	Found (µM)	Recovery (%)	RSD*
Orange juice	5.00 10.00 15.00	5.08 9.99 15.10	101.60 99.90 100.60	2.37 2.15 2.30
River water	5.00 10.00 15.00	5.02 9.98 15.04	100.40 99.80 100.20	2.56 2.32 2.60

*Measurement of three experiments (n=3).

4. CONCLUSION

In summary, $PrCoO_3$ compound were effectively synthesized in this study using a simple co-precipitation-assisted calcination process and were utilized to build an electrochemical sensor for sensitive and selective detection of CBZ in solution as well as in actual samples of orange juice and river water, with good results. The excellent performance of the present electrode was due to the high surface area of $PrCoO_3$ for CBZ adsorption, excellent conductivity, and fast electron transport. Moreover, the obtained results show the proposed electrochemical sensor exhibits good sensitivity 9.6619 μA μM^{-1} cm^{-2}, a wide linear range (0.001-84 μM), and an excellent limit of detection (LOD) 2 nM. Besides, the $PrCoO_3$ sensor revealed long-term stability and, good reproducibility as well as high selectivity, therefore the $PrCoO_3$ compound was promising sensor material to detect CBZ in real samples such as fruits, vegetables, soil, water, and pharmaceutical samples.

ACKNOWLEDGEMENT
The authors are grateful for the financial support from the Ministry of Science and Technology (MOST), Taiwan, Project no. MOST 107–2113-M-027–055-MY3.

References:

1. S. Singh, N. Singh, V. Kumar, S. Datta, A.B. Wani, D. Singh, K. Singh, J. Singh, *Environ. Chem. Lett.*, 14 (2016) 317–329.
2. S. Merel, S. Benzing, C. Gleiser, G. Di Napoli-Davis, C. Zwiener, *Environ. Pollut.*, 239 (2018) 512–521.
3. S. Verma, A. Srivastava, *Environ. Monit. Assess.*, 190 (2018).
4. Y.S. Wang, Y.J. Huang, W.C. Chen, J.H. Yen, *J. Hazard. Mater.*, 172 (2009) 84–91.
5. N. Liu, F. Dong, X. Liu, J. Xu, Y. Li, Y. Han, Y. Zhu, Y. Cheng, Z. Chen, Y. Tao, Y. Zheng, *Food Control*, 43 (2014) 115–120.
6. R.M. de Souza, D. Seibert, H.B. Quesada, F. de Jesus Bassetti, M.R. Fagundes-Klen, R. Bergamasco, *Process Saf. Environ. Prot.*, 135 (2020) 22–37.
7. X. Xu, J. Chen, B. Li, L. Tang, *Food Control*, 91 (2018) 20–25.
8. K.S. Bentley, D. Kirkland, M. Murphy, R. Marshall, *Mutat. Res. - Genet. Toxicol. Environ. Mutagen.*, 464 (2000) 41–51.
9. H. Li, H. du, L. Fang, Z. Dong, S. Guan, W. Fan, Z. Chen, *Regul. Toxicol. Pharmacol.*, 77 (2016) 200–205.
10. G. Ekstrom, M. Akerblom, *Rev. Environ. Contam. Toxicol.*, 114 (1990) 23–55.
11. K.R. Hakeem, M.S. Akhtar, S.N.A. Abdullah, *Plant, Soil Microbes Vol. 1 Implic. Crop Sci.* (2016) 1–366.
12. Q. Wu, Y. Li, C. Wang, Z. Liu, X. Zang, X. Zhou, Z. Wang, *Anal. Chim. Acta*, 638 (2009) 139–145.
13. M. Marinas, E. Sa, M.M. Rojas, M. Moalem, F.J. Urbano, C. Guillou, L. Rallo, *Rapid Commun. Mass Spectrom.*, 24 (2010) 1457–1466.
14. Y. Yang, D. Huo, H. Wu, X. Wang, J. Yang, M. Bian, Y. Ma, C. Hou, *Sensors Actuators, B Chem.*, 274 (2018) 296–303.
15. C. Zhu, D. Liu, Z. Chen, L. Li, T. You, *J. Colloid Interface Sci.*, 546 (2019) 92–100.
16. Y. Yang, X. Xing, T. Zou, Z. Wang, R. Zhao, P. Hong, S. Peng, X. Zhang, Y. Wang, *J. Hazard. Mater.*, 386 (2020) 121958.

17. G.M. Patel, J. V. Rohit, R.K. Singhal, S.K. Kailasa, *Sensors Actuators, B Chem.*, 206 (2015) 684–691.
18. N. Pourreza, S. Rastegarzadeh, A. Larki, *Talanta*, 134 (2015) 24–29.
19. T.W. Chen, R. Ramachandran, S.M. Chen, N. Kavitha, K. Dinakaran, R. Kannan, G. Anushya, N. Bhuvana, T. Jeyapragasam, V. Mariyappan, S.D. Rani, S. Chitra, *Catalysts*, 10 (2020) 1–23.
20. Y. Guo, S. Guo, J. Li, E. Wang, S. Dong, *Talanta*, 84 (2011) 60–64.
21. X. Liao, Z. Huang, K. Huang, M. Qiu, F. Chen, Y. Zhang, Y. Wen, J. Chen, *J. Electrochem. Soc.*, 166 (2019) B322–B327.
22. T.W. Chen, R. Ramachandran, S.M. Chen, G. Anushya, S.D. Rani, V. Mariyappan, P. Elumalai, N. Vasimalai, *Nanomaterials*, 11 (2021).
23. J.G. Bednorz, K.A. Müller, *Angew. Chemie Int. Ed. English*, 27 (1988) 735–748.
24. M. V. Kovalenko, L. Protesescu, M.I. Bodnarchuk, *Science (80-.).*, 358 (2017) 745–750.
25. T. Harigai, S.M. Nam, H. Kakemoto, S. Wada, K. Saito, T. Tsurumi, *Thin Solid Films*, 509 (2006) 13–17.
26. H. Hayashi, H. Inaba, M. Matsuyama, N.G. Lan, M. Dokiya, H. Tagawa, *Solid State Ionics*, 122 (1999) 1–15.
27. S.J. Skinner, *Int. J. Inorg. Mater.*, 3 (2001) 113–121.
28. J. Tong, W. Yang, B. Zhu, R. Cai, 203 (2002) 175–189.
29. H. Obayashi, Y. Sakurai, T. Gejo, *J. Solid State Chem.*, 17 (1976) 299–303.
30. N. Labhasetwar, G. Saravanan, S. Kumar Megarajan, N. Manwar, R. Khobragade, P. Doggali, F. Grasset, *Sci. Technol. Adv. Mater.*, 16 (2015) 1–13.
31. P.E. Marti, A. Baiker, *Catal. Letters*, 26 (1994) 71–84.
32. M. McIlvried, G. McCarthy, *Penn State University: University Park, PA, USA* 1973, 25-828.
33. A. Fujimori, J. Osterwalder, *J. Phys. C Solid State Phys.*, 17 (1984) 2869–2878.
34. G. Yin, X. Yuan, X. Du, W. Zhao, Q. Bi, F. Huang, *Chem. - A Eur. J.*, 24 (2018) 2157–2163.
35. A. Artemenko, A. Shchukarev, P. Štenclová, T. Wagberg, J. Segervald, X. Jia, A. Kromka, *IOP Conf.* Ser. Mater. Sci. *Eng.*, 1050 (2021).
36. S. Periyasamy, J. Vinoth Kumar, S.M. Chen, Y. Annamalai, R. Karthik, N. Erumaipatty Rajagounder, *ACS Appl. Mater. Interfaces*, 11 (2019) 37172–37183.
37. Y. Dong, L. Yang, L. Zhang, *J. Agric. Food Chem.*, 65 (2017) 727–736.
38. P. Wei, T. Gan, K. Wu, *Sensors Actuators, B Chem.*, 274 (2018) 551–559.
39. A. Özcan, F. Hamid, A.A. Özcan, *Talanta*, 222 (2021).
40. T. Kokulnathan, S.M. Chen, *ACS Appl. Mater. Interfaces*, 12 (2020) 16216–16226.
41. Y. Dong, J. Yang, X. Liu, L. Zhang, *J. Electrochem. Soc.*, 163 (2016) B652–B658.
42. X. Tu, F. Gao, X. Ma, J. Zou, Y. Yu, M. Li, F. Qu, X. Huang, L. Lu, *J. Hazard. Mater.*, 396 (2020) 122776.
43. Y. Zhou, Y. Li, P. Han, Y. Dang, M. Zhu, Q. Li, Y. Fu, *New J. Chem.*, 43 (2019) 14009–14019.